Rapid Communications

Modeling the universal viscoelastic response of polymer fibers

Aakash Sharma and Guruswamy Kumaraswamy*
Complex Fluids and Polymer Engineering Group, Polymer Science and Engineering Division, CSIR-National Chemical Laboratory, Dr. Homi Bhabha Road, Pune 411008, Maharashtra, India

Shirish Thakre
Fiber and Textiles, Aditya Birla Science and Technology Company Pvt. Ltd., Plot no. 1 and 1A/1 MIDC Taloja, Taluka Panvel, District Raigad 410208, Maharashtra, India

(Received 10 November 2017; published 20 June 2018)

Polymer fibers, including natural silk and synthetic fibers, exhibit universal viscoelastic response. On stretching below yield, they show logarithmic stress decay. On unloading fibers with a glassy amorphous phase, the stress recovers. A simple phenomenological model accurately describes data from independent mechanical experiments and provides insights into the microstructural origins of the fiber response. Counter to intuition, the model indicates that it is the crystalline regions, rather than the amorphous glass, that deform first on stretching fibers at high strain rates. On holding a stretched fiber, stress decays as a consequence of relaxations in amorphous regions. Finally, unloading the fiber transfers stress from the amorphous to crystalline regions resulting in stress recovery. Model parameters correlate well with the fiber microstructure. Crystal and amorphous moduli from the model match those from x-ray diffraction. Activation energies for the temperature dependence of the peak relaxation time are similar to those reported in the literature. Thus, a simple model that invokes only crystal-amorphous coexistence can successfully model the mechanical response of a wide variety of polymer fibers.

DOI: 10.1103/PhysRevMaterials.2.062601

Polymer fibers are ubiquitous in nature (for example, silk or cellulosic plant fibers) as well as in industrial practice (for example, PET or nylon). The toughness of natural silks and the springiness of synthetic fibers woven into carpets are determined by the fiber microstructure [1–6]. A majority of polymer fibers, including silk and PET, are semicrystalline. Such polymers have a regular chemical structure that allows them to crystallize. However, the long chain nature of polymer molecules precludes complete crystallization and amorphous and crystal phases coexist in the semicrystalline state. Two phase coexistence over a wide range of temperature and pressure violates the Gibbs rule and is indicative of the nonequilibrium nature of semicrystalline polymers. Further, at temperatures below the glass transition temperature (T_g) of the polymer, the amorphous phase is glassy.

Modelling the mechanical response of semicrystalline polymer fibers is challenging due to their structural complexity. Polymers crystallize to form lamellae that are tens of nanometers thick. Since the thickness of the lamellar crystal is much smaller than the typical polymer contour length, a polymer chain spans multiple lamellae [7]. Parts of a chain that are between crystalline lamellae are in the amorphous state. Further complexity, such as the presence of microvoids or a core-shell structure might arise from the spinning process that produces the fiber. Thus, semicrystalline microstructure is characterized by ordering over a wide range of length scales, making it difficult to develop tractable molecular models to capture their behavior. Several attempts have been made over the last several decades to develop phenomenological models for the viscoelastic response of polymer fibers [8–12]. For example, the response of silk fibers to cyclic loading has recently been modelled [10]. However, this model is incapable of capturing stress recovery observed on unloading silk fibers. Phenomenological models have also been developed that capture the response of polyethylene fibers [8,13]. Here, we demonstrate that a wide variety of semicrystalline polymer fibers, including natural and synthetic fibers, exhibit universal viscoelastic response. We present a phenomenological model, that is independent of fiber chemistry, that captures data from independent mechanical experiments and offers insights into the microstructural origins of the mechanical response.

We examine semicrystalline polymer fibers of polyacrylonitrile (PAN), polyethyleneterephthalate (PET), regenerated cellulose, and silk fibroin. PAN and PET fibers are synthetic whereas regenerated cellulose is obtained from natural cellulose [14–16]. Silk is a natural fiber obtained from silkworms [17,18]. At room temperature, PET, PAN, regenerated cellulose, and silk fibroin have a glassy amorphous phase. Thus, our experiments investigate synthetic as well as natural semicrystalline polymer fibers, prepared using a wide range of spinning methods (including solution and melt spinning and reactive regeneration).

We isolate individual fibers and stretch them at a constant rate ($=4 \times 10^{-3}$ s^{-1}) to investigate their stress-strain response [Fig. 1(a)]. Experimental details are provided in the Supplemental Material [19,20]. Briefly, we clamp the ends of a fiber and stretch them in a rheometer. Each measurement was repeated on at least 10 independent fibers. Variation in the data across fibers was less than 10%. Here, representative

*g.kumaraswamy@ncl.res.in

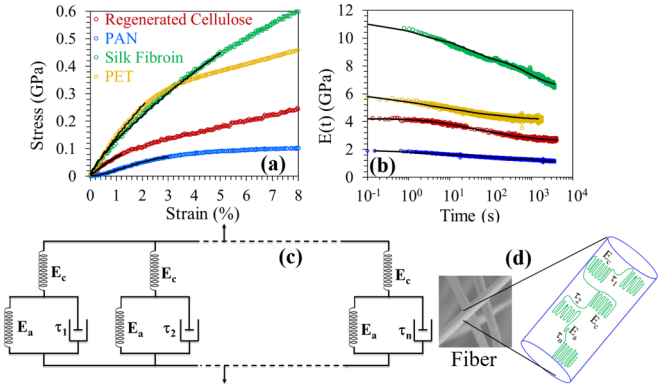

FIG. 1. (a) Stress strain response from various semicrystalline fibers at a constant stretch rate of 4×10^{-3} s^{-1}. The yield strain ϵ_y for Cellulose, PAN, PET, and silk fibers was determined to be 1.3%, 3.5%, 2.1%, and 7.6%, respectively. (b) Modulus, $E(t) = \sigma(t)/\epsilon_o$ from stress relaxation experiments for fibers held after stretching to a strain, $\epsilon_o < \epsilon_y$. The black lines represent fits to the model shown in (c) comprising units with an elastic element in series with a Kelvin Voigt element. We assume a distribution of relaxation times in each unit that is represented schematically as a parallel combination. (d) Schematic representation of polymer chains spanning crystalline lamellae and amorphous domains in the semicrystalline fibers.

data from one fiber is presented. At low strains, the stress is linear in strain for all fibers [Fig. 1(a)]. We observe that the fibers yield at a critical strain ϵ_y, above which the slope of the stress-strain data decreases. For strains $<\epsilon_y$, stress-strain data is reversible, viz. the stress decreases to zero along the same path on unloading the fiber immediately after stretching. Above ϵ_y, there is permanent deformation of the fiber and we observe a residual plastic strain on unloading the fiber to zero stress immediately after stretching (Supplemental Material Fig. 1 [19]). The elastic response of the fibers below ϵ_y is characteristic of the microstructure of the as spun fiber and is independent of the strain rate (Supplemental Material Fig. 2 [19]). Here, we restrict our investigations to the elastic response region.

Polymer fibers are viscoelastic. We investigate the fiber viscoelastic response by performing stress relaxation experiments. Here, a fiber is stretched (at 4×10^{-3} s^{-1}) to a strain below the yield strain and the stress is monitored while holding the fiber at that strain. For all semicrystalline fibers, the stress decays logarithmically with time [Fig. 1(b)]. The stress does not decay to zero even after holding for several days. The logarithmic time decay of stress suggests that relaxation is governed by processes characterized by widely varying time scales.

We describe the mechanical response of the fibers using a phenomenological model as shown schematically in Fig. 1(c). Each unit comprises a Kelvin-Voigt element (with elastic modulus E_a and relaxation time τ) in series with an elastic spring with modulus E_c. This unit is described by the following equation:

$$\frac{d\sigma}{dt} + \frac{\sigma}{\tau} - \frac{E_c E_a}{\tau(E_c + E_a)}\epsilon - E_c\frac{d\epsilon}{dt} = 0. \quad (1)$$

TABLE I. Moduli from fitting and WAXD.

		Moduli from fitting (Pa)	Moduli from WAXD (Pa)
Regenerated cellulose	E_c	1.25×10^{10}	1.42×10^{10}
	E_a	1.1×10^{9}	1.78×10^{9}
Silk fibroin	E_c	1.3×10^{10}	1.16×10^{10}
	E_a	4.57×10^{9}	4.96×10^{9}
PET	E_c	6.06×10^{9}	5.81×10^{9}
	E_a	2.27×10^{9}	2.32×10^{9}
PAN	E_c	2.17×10^{9}	
	E_a	4.44×10^{8}	

Since the polymer fibers exhibit logarithmic stress decay, we model the response using a spectrum of relaxation times, $P(\tau)$, corresponding to the spatial heterogeneity of the amorphous domains [Fig. 1(d)]. From equation (1), we obtain the stress developed, σ_{s-s}, on stretching the fiber at a constant strain rate $\bar{\epsilon}$ and the time-dependent stress relaxation (σ_r) as:

$$\sigma_{s-s} = \int_{-\infty}^{\infty} P(\tau)\frac{E_c}{E_c + E_a}[E_a\epsilon + E_c\tau\bar{\epsilon}(1 - e^{-\frac{t}{\tau}})]d\tau \quad (2)$$

$$\sigma_r = \int_{-\infty}^{\infty} P(\tau)\left\{\left[\sigma_o - \frac{E_c E_a \epsilon}{E_c + E_a}\right]e^{-\frac{t}{\tau}} + \frac{E_c E_a \epsilon}{E_c + E_a}\right\}d\tau. \quad (3)$$

For $E_a > 0$, the stress from this model never decays to zero during stress relaxation experiments.

Fiber stretching and stress relaxation are independent experiments. We obtain the fit parameters, E_c, E_a, and $P(\tau)$ by simultaneously fitting the model to data from these two independent experiments using CONTIN regularization [21,22]. Since we simultaneously fit stress-strain and stress relaxation data, the model converges robustly to the same fit parameters even with widely varying initial guesses. Fit parameters E_c and E_a are given in Table I and the relaxation spectra $P(\tau)$ are shown in Fig. 2. In all fibers, $E_c > E_a$. As anticipated from the stress decay data, $P(\tau)$ varies widely (Fig. 2). We observe that $P(\tau)$ is monomodal for PET, PAN, and silk and is bimodal for the regenerated cellulose fibers.

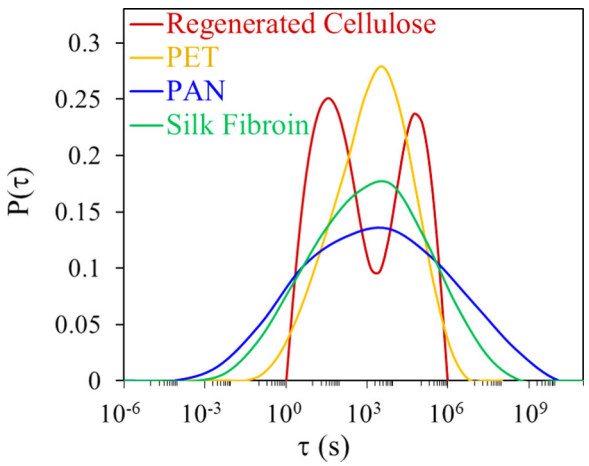

FIG. 2. The best fit for the relaxation times, $P(\tau)$, obtained by fitting the experimental data to the model.

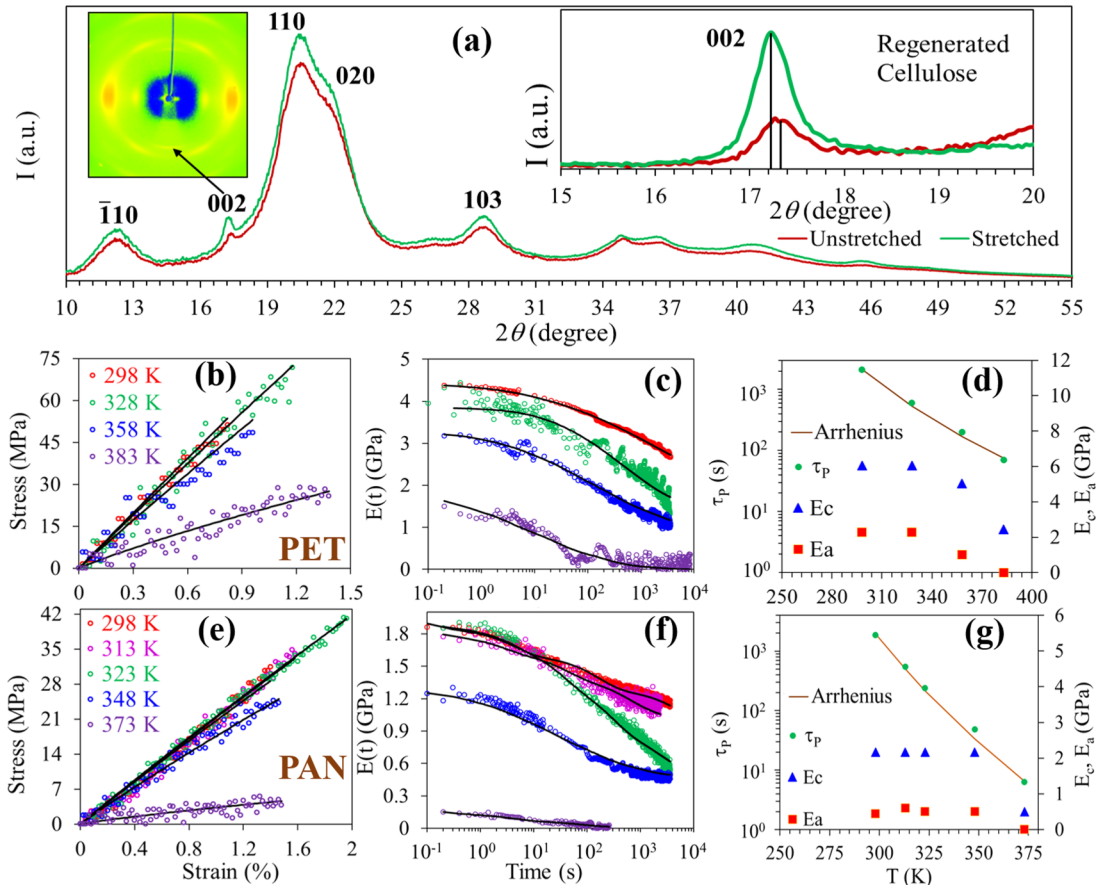

FIG. 3. (a) Wide angle x-ray diffraction data for regenerated cellulose fiber in unstretched and stretched states. 2D data obtained from the WAXD is shown as an inset (left). The data are reduced to 1D (intensity versus 2θ) by circular averaging. WAXD peaks were indexed based on the literature [31,32]. The inset on the right clearly shows that the 002 peak shifts to lower 2θ upon stretching. Data for PET and PAN fibers are shown in the middle and bottom, respectively. (b),(e) Stress strain and (c),(f) stress relaxation experiments performed at temperatures of 298, 328, 358, and 383 K for PET and 298, 313, 323, 348, and 373 K for PAN fibers. Fits to the data are indicated as black lines. Temperature dependent model parameters are given in (d,g).

We now explore how these model parameters relate to the semicrystalline microstructure. Since $E_c > E_a$, it is possible that E_c represents the elastic modulus of the crystalline domains while E_a represents the low strain elastic response of the glassy amorphous domains. To verify this, we employ wide angle x-ray diffraction (WAXD) to independently estimate the elastic moduli associated with the crystalline and glassy amorphous domains.

We cannot perform WAXD on a single fiber. Therefore, we perform in-situ WAXD on a bunch of fibers stretched to strains below ϵ_y in a stretching device. The fiber spinning process induces strong uniaxial orientation in the crystalline phase, reflected in 2D-WAXD from aligned fibers. We perform WAXD on fibers that are held in the stretched state for two days, such that the stress approaches a steady state. The meridional WAXD peaks shift to lower 2θ when fibers are stretched. For example, we show the shift for the 002 peak on stretching regenerated cellulose fibers [Fig. 3(a)]. From the WAXD peak positions, we can calculate crystalline unit cell parameters for unstretched and stretched fibers. We observe that stretching induces an extension of the crystal unit cell along the c axis and a small compression along the a and b axes (details in Supplemental Material [19]). Since the polymer chain is aligned along the c axis of the crystalline unit cell [23], stretching results in elongation of the polymer crystals along the chain axis. We calculate the crystalline strain, $\epsilon_c (= \frac{\Delta c}{c})$, as the ratio of the change along the c axis, normalized by the unstretched unit cell distance along the c axis. It is well established in literature that the stress is homogeneously distributed on the crystal and amorphous parts of semicrystalline polymers [24–26]. Hence, crystalline and amorphous phases have been modelled as two springs connected in series by Dulmage and Sakurada [27–30]. We modify their method to estimate the strain on the amorphous regions as $\epsilon_a = \epsilon - \epsilon_c$. At steady state, the stress corresponds to a series combination of the crystalline and glassy elastic elements. Thus, $\sigma = \frac{E_c E_a \epsilon}{E_c + E_a}$. Therefore, we calculate the elastic moduli as:

$$E_c = \frac{\sigma}{\epsilon_c} \quad E_a = \frac{\sigma}{\epsilon_a}. \tag{4}$$

We use this method to estimate the elastic moduli for PET, silk, and regenerated cellulose fibers. PAN fibers show only equatorial peaks (200) and (310): Therefore, it is not possible to obtain the unit cell dimension along the c axis from WAXD and, we cannot use this method to estimate the elastic modulus for PAN fibers. The moduli, E_c and E_a, obtained from

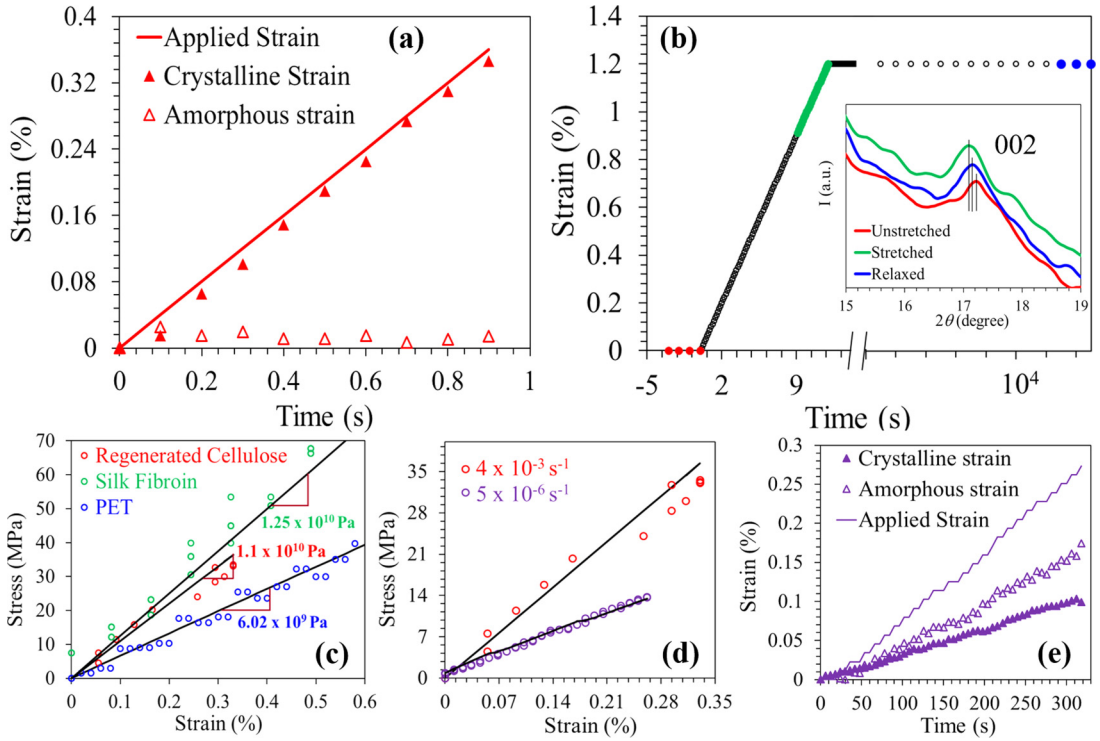

FIG. 4. (a) Evolution of crystalline and amorphous strains from the model during stretching of cellulose fibers at 4×10^{-3} s^{-1}. (b) Variation of strain with time for cellulose fibers shows three regions where WAXD (shown in inset) is performed: Red (unstretched fibers), green (during stretching), and blue (relaxed fibers). (c) Initial slope of the stress vs strain curve for regenerated cellulose, PET, and silk fibers obtained at 4×10^{-3} s^{-1} [compare with the crystal modulus obtained from WAXD (Table I)]. (d) Stress vs strain data for cellulose fibers stretched at (4×10^{-3} s^{-1}) and at extremely low strain rate (5×10^{-6} s^{-1}). (e) Evolution of crystalline and amorphous strains from model during stretching of cellulose fibers at (5×10^{-6} s^{-1}) [compare with (a)].

WAXD for PET, silk, and regenerated cellulose fibers agree reasonably well with those from the model fits (see Table I). This supports our assumption that E_c and E_a obtained from the model can be interpreted as the elastic moduli corresponding to crystalline and amorphous domains of the semicrystalline fibers, respectively.

We now examine the temperature dependence of the model parameters, $P(\tau)$, E_c, and E_a, as PET and PAN fibers are heated to temperatures approaching their T_g. Fiber orientation results in an increase in the T_g for fibers. We measure T_g of 375 K and 389 K for PAN and PET fibers, respectively—higher than literature values for unoriented samples (PET—353 K, PAN—369 K). On heating PAN and PET fibers from 298 K to near T_g, there is a systematic decrease in the fiber modulus, suggesting softening of fibers with temperature [Figs. 3(b) and 3(e)]. Correspondingly, model fits to the data show a two- to fivefold decrease in E_c on approaching T_g. In contrast, near the polymer T_g there is a qualitative change in the stress relaxation for both fibers. Near T_g, the stress in both PET and PAN stretched fibers decreases to 0 upon holding for about 1000 s. Correspondingly, E_a decreases abruptly to 0 near T_g [Figs. 3(c) and 3(f)]. Thus, the mechanical response of PET and PAN fibers on approaching the amorphous phase T_g is described by a simple Maxwell model comprising an elastic element in series with a viscous element [33]. The behavior of E_a close to T_g is further evidence that E_a is related to the response of the amorphous domains.

On heating, there is also a shift in $P(\tau)$ to lower values (Supplemental Material Fig. 3 [19]). We plot the temperature dependent decrease in the peak of the relaxation time distribution, τ_P [Figs. 3(d) and 3(g)]. There is an exponential decrease in τ_P with temperature, characterized by an activation energy of 37.4 kJ/mol for PET and 70.2 kJ/mol for PAN. We note that these values for the activation energy compare favorably with those from dielectric measurements of β relaxation processes in these material [34,35]. Further, dielectric measurements yield broad relaxation spectra corresponding to β processes, comparable to the breadth of $P(\tau)$ from our model fits (PET [36,37], PAN [38], regenerated cellulose [39]). Thus, the amorphous relaxations that we obtain from our model correlate with sub- T_g motions reported for these polymers. Thus, the parameters of this simple model bear a remarkable correspondence with the microstructural features of semicrystalline fibers: The moduli correspond to the elastic response of crystalline and amorphous phases while the relaxation time spectra represent the contribution of sub-T_g processes in the amorphous regions.

Having established the connection between the model and semicrystalline microstructure, we now explore the predictions of the model. We calculate the strain in the crystalline and amorphous domains when regenerated cellulose fibers are stretched at 4×10^{-3} s^{-1}, using the model parameters calculated earlier. Counter to intuition, the model suggests that it is the crystalline regions that deform, and that there is no deformation of the glassy amorphous regions during

stretching as shown in Fig. 4(a) (see Supplemental Material Fig. 4 [19] for all fibers). The time scales for the stretching experiment ($\dot{\epsilon}^{-1} = 250$ s) is significantly smaller than those that characterize glassy relaxation (Fig. 2). Thus, the glassy amorphous phase is unable to respond during stretching and it is only the crystalline regions that get strained. We now present three independent experiments that support this surprising prediction of the model.

At first, we use WAXD to directly examine the crystalline strain when the cellulose fibers are stretched. We stretch cellulose fibers to a strain of 1.2% ($<\epsilon_y$) and obtain WAXD data for 3 s, close to the peak strain [Fig. 4(b)]. Since, the data acquisition time is small, we average data over five repeat measurements to improve signal to noise. Then, we allow the fibers to relax over two days and obtain WAXD at steady state. We observe that the crystal expands in the c-axis direction during stretching and subsequently shrinks as stress is transferred to the amorphous glassy phase during relaxation. This provides direct proof for deformation of the crystalline phase during stretching. We note that crystal deformation happens during stretching only for semicrystalline samples with a glassy amorphous phase, for which our model is valid. When we stretch fibers of high molecular weight polyethylene, where the amorphous phase is rubbery, we observe no change in the position of the meridional peak in WAXD (see Supplemental Material Fig. 5 [19,40]). Next, we examine the slope of the stress-strain data during stretching and compare with the crystalline modulus obtained directly from WAXD measurements. We observe that for regenerated cellulose, PET, and silk fibroin stretched at 4×10^{-3} s^{-1}, the slope of the stress-strain curve as shown in Fig. 4(c) is approximately equal to the crystalline modulus obtained from WAXD in Table I. Thus, the modulus obtained by stretching a composite structure comprised of interconnected crystalline and amorphous domains closely matches the crystalline modulus obtained independently from WAXD measurements. This strongly suggests that it is indeed the crystal regions that deform during stretching of semicrystalline fibers with a glassy amorphous phase. Finally, the model suggests that if we stretch the fibers at extremely low strain rates, then there will also be a contribution of the amorphous phase to the mechanical response. Here, the strain rates should be sufficiently low such that the time scale that characterizes deformation is comparable to the slowest relaxation times of the amorphous phase. We perform stretching experiments on regenerated cellulose fibers at a strain rate of 5×10^{-6} s^{-1}, three orders of magnitude lower than that in our previous experiments. We observe that the initial slope of the stress strain curve is lower than at higher strain rates (and therefore lower than the crystalline modulus [Fig. 4(d)]). Using the model parameters obtained previously, we observe that in this experiment, the strain is taken up by both amorphous and crystalline regions [Fig. 4(e)]. Thus, taken together, our data provide strong evidence for the nonintuitive predictions of the model.

In semicrystalline fibers where glassy amorphous domains are modelled as Voigt elements, stress relaxation does not correspond to irrecoverable viscous dissipation. Our model predicts that as strain is transferred to the glassy amorphous domains, the energy during stress relaxation is not lost. Rather, it is stored in the elastic component (E_a) of the Voigt element.

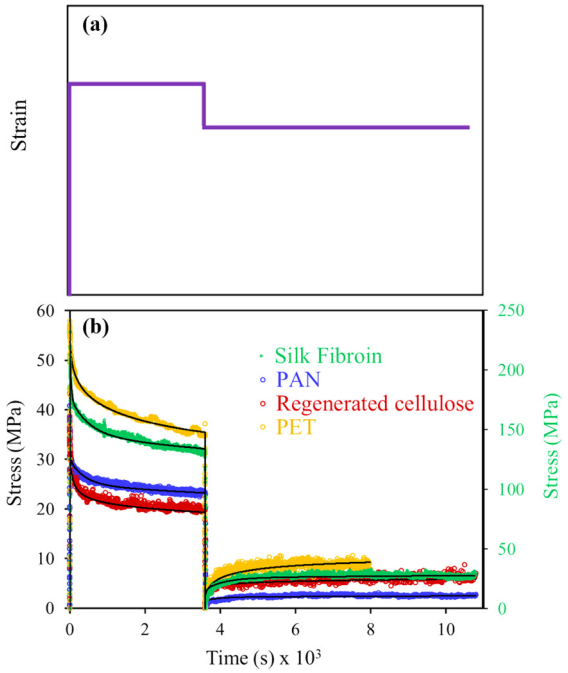

FIG. 5. (a) Experimental protocol for strain imposed during stress recovery experiments. (b) The response from fibers with glassy amorphous phase shows recovery in stress after relaxation.

This should result in an internal buildup of stress in the fiber. Thus, if the fiber is unloaded to zero stress after stress relaxation, then this internal builtup stress in the amorphous domain is transferred back to the crystalline domain, that should manifest as an increase in the fiber stress over the slow time scales that characterize the glassy amorphous phase.

To verify this prediction, we performed stress recovery experiments. Here, semicrystalline fibers with a glassy amorphous phase are stretched below yield and are allowed to relax for 3600 s. Then the fiber is unloaded by rapidly reducing strain (at 4×10^{-3} s^{-1}), until the stress decreases to zero. Stress decreases to zero at nonzero strain, as anticipated by the model. The fibers are then held at this strain and the stress is monitored [Fig. 5(a)]. For all semicrystalline fibers investigated: PET, PAN, silk, and regenerated cellulose fibers, we observe an increase in stress with time as shown in Fig. 5(b). Further, the increase in stress is quantitatively predicted by the model using the same parameters obtained from fitting the stress-strain and stress relaxation data. The model fit is shown as a black line in Fig. 5(b). Where $E_a = 0$, e.g., PET and PAN near T_g, those fibers do not show stress recovery.

Thus, we have demonstrated that a relatively simple model can quantitatively capture the mechanical response of a wide variety of semicrystalline fibers, for independent measurements (stress-strain, stress relaxation, and recovery) and over a wide temperature range. To the best of our knowledge, none of the models reported in the literature capture the response from such diverse experiments for different polymers [41–46]. Our model predicts the mechanical response of synthetic fibers (PET, PAN, regenerated cellulose) with different chemistries, manufactured using a wide variety of spinning processes, as well as of natural fibers (silk). These fibers

exhibit wide variations in crystallinity, orientation, and morphology. For example, reactively regenerated viscose cellulose fibers are characterized by an amorphous skin/crystalline core morphology, while other fibers do not show such dramatic radial variation. We do not account for such morphological differences—the fiber response is modelled as arising only from the amorphous/crystal connectivity in the semicrystalline microstructure. This appears to be sufficient to describe the mechanical response of the fibers. Further, model parameters are constrained by simultaneously fitting independent experiment results. These model parameters correlate to the semicrystalline microstructure in a physically meaningful way and fitted values match reasonably well with those from WAXD experiments and literature.

A.S. acknowledges Aditya Birla Science and Technology Company Pvt. Ltd. for funding and Dr. Anuya Nisal for providing silk fibers.

[1] I. M. Ward, *Structure and Properties of Oriented Polymers* (Springer Science & Business Media, Essex, England, 2012).
[2] M. Northolt, Polymer **21**, 1199 (1980).
[3] J. Cai, L. Zhang, J. Zhou, H. Qi, H. Chen, T. Kondo, X. Chen, and B. Chu, Adv. Mater. **19**, 821 (2007).
[4] K. Kong, R. J. Davies, M. A. McDonald, R. J. Young, M. A. Wilding, R. N. Ibbett, and S. J. Eichhorn, Biomacromolecules **8**, 624 (2007).
[5] S. Jabbari-Farouji, O. Lame, M. Perez, J. Rottler, and J.-L. Barrat, Phys. Rev. Lett. **118**, 217802 (2017).
[6] J. Che, C. R. Locker, S. Lee, G. C. Rutledge, B. S. Hsiao, and A. H. Tsou, Macromolecules **46**, 5279 (2013).
[7] B. S. Hsiao, L. Yang, R. H. Somani, C. A. Avila-Orta, and L. Zhu, Phys. Rev. Lett. **94**, 117802 (2005).
[8] M. Wilding and I. Ward, J. Mater. Sci. **19**, 629 (1984).
[9] F. Shi, Fibres & Textiles in Eastern Europe **21**, 51 (2013).
[10] I. Krasnov, I. Diddens, N. Hauptmann, G. Helms, M. Ogurreck, T. Seydel, S. S. Funari, and M. Müller, Phys. Rev. Lett. **100**, 048104 (2008).
[11] I. Krasnov, T. Seydel, and M. Müller, Phys. Rev. E **91**, 042716 (2015).
[12] A. Manich, P. Marino, M. De Castellar, M. Saldivia, and R. Sauri, J. Appl. Polym. Sci. **76**, 2062 (2000).
[13] V. Djokovic, D. Kostoski, S. Galovic, M. Dramicanin, and Z. Kacarevic-Popovic, Polymer **40**, 2631 (1999).
[14] E. A. Morris and M. C. Weisenberger, *Polymer Precursor-Derived Carbon* (ACS Publications, Washington DC, 2014), pp. 189–213.
[15] G.-Y. Chen, J. A. Cuculo, and P. A. Tucker, J. Appl. Polym. Sci. **44**, 447 (1992).
[16] C. Woodings, *Regenerated Cellulose Fibres*, Vol. 18 (Woodhead Publishing, Cambridge, 2001).
[17] H.-J. Jin and D. L. Kaplan, Nature (London) **424**, 1057 (2003).
[18] C. Fu, Z. Shao, and V. Fritz, Chem. Commun. 6515 (2009).
[19] See Supplemental Material at http://link.aps.org/supplemental/10.1103/PhysRevMaterials.2.062601 for methodology, lattice parameter calculations, stretching of fibers to different strains, dependence of yield strain on strain rate, dependence of relaxation time spectra on temperature, variation of crystalline and amorphous strains in different fibers with stretching, and effect of stretching on the meridional peak for polyethylene.
[20] R.-B. Adusumalli, U. Müller, H. Weber, T. Roeder, H. Sixta, and W. Gindl, in *Macromolecular Symposia*, Vol. 244 (Wiley Online Library, Wiesbaden, 2006), pp. 83–88.
[21] S. W. Provencher, Comput. Phys. Commun. **27**, 229 (1982).
[22] I.-G. Marino, *Regularized Inverse Laplace Transform*, MATLAB Central File Exchange, Retrieved September 03 2016 (2007) https://www.mathworks.com/matlabcentral/fileexchange/6523-rilt.
[23] P. Zugenmaier, Prog. Polym. Sci. **26**, 1341 (2001).
[24] J. Sirichaisit, V. L. Brookes, R. J. Young, and F. Vollrath, Biomacromolecules **4**, 387 (2003).
[25] W. Yeh and R. Young, Polymer **40**, 857 (1999).
[26] R. Young, J. Text. Inst. **86**, 360 (1995).
[27] W. J. Dulmage and L. E. Contois, J. Polym. Sci. **28**, 275 (1958).
[28] I. Sakurada, Y. Nukushina, and T. Ito, J. Polym. Sci. **57**, 651 (1962).
[29] I. Sakurada, T. Ito, and K. Nakamae, Macromol. Chem. Phys. **75**, 1 (1964).
[30] I. Satcurada, T. Ito, and K. Nakamae, in *Journal of Polymer Science: Polymer Symposia*, Vol. 15 (Wiley Online Library, Easton, 1967), pp. 75–91.
[31] G. Jiang, Y. Yuan, B. Wang, X. Yin, K. S. Mukuze, W. Huang, Y. Zhang, and H. Wang, Cellulose **19**, 1075 (2012).
[32] X. Chen, C. Burger, D. Fang, D. Ruan, L. Zhang, B. S. Hsiao, and B. Chu, Polymer **47**, 2839 (2006).
[33] I. M. Ward and J. Sweeney, *Mechanical Properties of Solid Polymers* (John Wiley & Sons, Chichester, 2012).
[34] A. Maxwell, L. Monnerie, and I. Ward, Polymer **39**, 6851 (1998).
[35] S. Okajima, M. Ikeda, and A. Takeuchi, J. Polym. Sci., Part A: Polym. Chem. **6**, 1925 (1968).
[36] E. Neagu, P. Pissis, L. Apekis, and J. G. Ribelles, J. Phys. D **30**, 1551 (1997).
[37] R. H. Boyd, Polymer **26**, 323 (1985).
[38] R. Hayakawa, T. Nishi, K. Arisawa, and Y. Wada, J. Polym. Sci., Part B: Polym. Phys. **5**, 165 (1967).
[39] J. Einfeldt, D. Meißner, and A. Kwasniewski, J. Non-Cryst. Solids **320**, 40 (2003).
[40] P. B. McDaniel, J. M. Deitzel, and J. W. Gillespie, Jr., Polymer **69**, 148 (2015).
[41] M. Kitagawa and H. Takagi, J. Polym. Sci., Part B: Polym. Phys. **28**, 1943 (1990).
[42] M. Kitagawa, T. Mori, and T. Matsutani, J. Polym. Sci., Part B: Polym. Phys. **27**, 85 (1989).
[43] K. Hong and G. Strobl, Macromolecules **39**, 268 (2006).
[44] Y. Men, J. Rieger, and G. Strobl, Phys. Rev. Lett. **91**, 095502 (2003).
[45] K. Hong, A. Rastogi, and G. Strobl, Macromolecules **37**, 10174 (2004).
[46] R. Haward and G. Thackray, in *Proceedings of the Royal Society of London A: Mathematical, Physical and Engineering Sciences*, Vol. 302 (The Royal Society, London, 1968), pp. 453–472.